

Alma Mater Studiorum Università di Bologna
Archivio istituzionale della ricerca

TUNING CYSTEINE REACTIVITY AND SULFENIC ACID STABILITY BY PROTEIN MICROENVIRONMENT IN
GLYCERALDEHYDE-3-PHOSPHATE DEHYDROGENASES OF ARABIDOPSIS THALIANA

This is the final peer-reviewed author's accepted manuscript (postprint) of the following publication:

Published Version:

Zaffagnini, M., Fermani, S., Calvaresi, M., Orrù, R., Iommarini, L., Sparla, F., et al. (2016). TUNING CYSTEINE REACTIVITY AND SULFENIC ACID STABILITY BY PROTEIN MICROENVIRONMENT IN GLYCERALDEHYDE-3-PHOSPHATE DEHYDROGENASES OF ARABIDOPSIS THALIANA. *ANTIOXIDANTS & REDOX SIGNALING*, 24, 502-517 [10.1089/ars.2015.6417].

Availability:

This version is available at: <https://hdl.handle.net/11585/551510> since: 2022-01-31

Published:

DOI: <http://doi.org/10.1089/ars.2015.6417>

Terms of use:

Some rights reserved. The terms and conditions for the reuse of this version of the manuscript are specified in the publishing policy. For all terms of use and more information see the publisher's website.

This item was downloaded from IRIS Università di Bologna (<https://cris.unibo.it/>).
When citing, please refer to the published version.

(Article begins on next page)

This is the final peer-reviewed accepted manuscript of:

M. Zaffagnini, S. Fermani, M. Calvaresi, R. Orrù, L. Iommarini, F. Sparla, G. Falini, A. Bottoni, P. Trost, "Tuning Cysteine Reactivity and Sulfenic Acid Stability by Protein Microenvironment in Glyceraldehyde-3-Phosphate Dehydrogenases of *Arabidopsis Thaliana*". *Antioxidants & Redox Signaling* (2016)

The final published version is available online at:
<https://www.liebertpub.com/doi/10.1089/ars.2015.6417>

Rights / License:

The terms and conditions for the reuse of this version of the manuscript are specified in the publishing policy. For all terms of use and more information see the publisher's website.

This item was downloaded from IRIS Università di Bologna (<https://cris.unibo.it/>)

When citing, please refer to the published version.

Tuning Cysteine Reactivity and Sulfenic Acid Stability by Protein Microenvironment in Glyceraldehyde-3-Phosphate Dehydrogenases of *Arabidopsis Thaliana*

Mirko Zaffagnini,^{1,*} Simona Fermani,^{2,*} Matteo Calvaresi,^{2,*} Roberto Orrù,¹ Luisa Iommarini,¹ Francesca Sparla,¹ Giuseppe Falini,² Andrea Bottoni,² and Paolo Trost¹

Abstract

Aims: Cysteines and H₂O₂ are fundamental players in redox signaling. Cysteine thiol deprotonation favors the reaction with H₂O₂ that generates sulfenic acids with dual electrophilic/nucleophilic nature. The protein microenvironment surrounding the target cysteine is believed to control whether sulfenic acid can be reversibly regulated by disulfide formation or irreversibly oxidized to sulfinates/sulfonates. In this study, we present experimental oxidation kinetics and a quantum mechanical/molecular mechanical (QM/MM) investigation to elucidate the reaction of H₂O₂ with glycolytic and photosynthetic glyceraldehyde-3-phosphate dehydrogenase from *Arabidopsis thaliana* (cytoplasmic AtGAPC1 and chloroplastic AtGAPA, respectively). **Results:** Although AtGAPC1 and AtGAPA have almost identical 3D structure and similar acidity of their catalytic Cys149, AtGAPC1 is more sensitive to H₂O₂ and prone to irreversible oxidation than AtGAPA. As a result, sulfenic acid is more stable in AtGAPA. **Innovation:** Based on crystallographic structures of AtGAPC1 and AtGAPA, the reaction potential energy surface for Cys149 oxidation by H₂O₂ was calculated by QM. In both enzymes, sulfenic acid formation was characterized by a lower energy barrier than sulfinic acid formation, and sulfonate formation was prevented by very high energy barriers. Activation energies for both oxidation steps were lower in AtGAPC1 than AtGAPA, supporting the higher propensity of AtGAPC1 toward irreversible oxidation. **Conclusions:** QM/MM calculations coupled to fingerprinting analyses revealed that two Arg of AtGAPA (substituted by Gly and Val in AtGAPC1), located at 8–15 Å distance from Cys149, are the major factors responsible for sulfenic acid stability, underpinning the importance of long-distance polar interactions in tuning sulfenic acid stability in native protein microenvironments.

Introduction

REACTIVE OXYGEN SPECIES (ROS) are unavoidable by-products of aerobic life, and plant cells may generate ROS by several means, under both physiological and pathological conditions (43, 50). Besides ROS generation by respiratory complexes, similar in animal and plant mitochondria, plant cells may produce ROS as a consequence of photosynthetic activity. Although ROS generated by the different photosystems may be dissimilar, for example, singlet oxygen by photosystem II and superoxide by photosystem I, only hydrogen peroxide (H₂O₂), which results from dismutation of superoxide,

is a long-living ROS that may accumulate in plant cells to micromolar levels or more (42, 51). Within cells, H₂O₂ reacts primarily with metal redox centers (e.g., heme iron of ascorbate peroxidase or catalase) and acidic protein thiols (44, 47). In particular, H₂O₂ and protein-reactive cysteines are fundamental molecules of redox signaling networks in plant cells (38, 48, 60, 64). H₂O₂ molecules may undergo the nucleophilic attack of a thiolate (S⁻) to give rise to sulfenic acid (-SOH) as a primary oxidation product (Fig. 1), which plays a pivotal role in redox signaling networks thanks to its dual nature of electrophile and nucleophile (7, 34, 44). On the contrary, protonated thiols (-SH) are unable to perform this reaction at significant rates.

Departments of ¹Pharmacy and Biotechnology and ²Chemistry “G. Ciamician,” University of Bologna, Bologna, Italy.

*These authors contributed equally to this work.

Innovation

Cysteine sulfenic acids are the primary products of H_2O_2 -dependent oxidation of protein thiolates and play an essential role in redox signaling. Glycolytic and photosynthetic glyceraldehyde-3-phosphate dehydrogenases (GAPDHs) are very similar proteins with different sensitivity to H_2O_2 . Since cysteine reactivity depends on the protein microenvironment, GAPDHs are ideal candidates for a thorough analysis of the structural determinants of sulfenic acid stability in real proteins. Based on biochemical and computational analyses, we demonstrate that long-distance polar interactions involving few selected amino acids determine the fate of GAPDH catalytic cysteines upon oxidation by H_2O_2 and hence their potential role in redox signaling.

The relationship between cysteine reactivity and its acidity is not obvious. Free cysteine has an ionization constant (pK_a) of 8.6 and the cysteine of glutathione is only slightly more acidic (8.3), but a restricted number of protein cysteines show much lower pK_a values (e.g., pK_a 4–7). Among the major factors that may locally favor thiol ionization in proteins, there are positively charged amino acids and hydrogen bond networks engaging the thiolate. Location of the cysteine at the *N*-terminus of an α -helix may also contribute to its acidity *via* helix macrodipole (32, 49). However, although ionization is a prerequisite for thiol reactivity with H_2O_2 , the nucleophilicity of thiolates decreases with decreasing of the pK_a of the corresponding thiols (21). Therefore, very acidic cysteines may be less reactive toward H_2O_2 than less acidic ones, provided that both are essentially deprotonated at physiological pH.

Peroxiredoxins (PRXs), which are specifically optimized for scavenging H_2O_2 within cellular environments, represent a special case since their activity is based on a moderately acidic (pK_a 5.2–5.8), but extremely reactive, cysteine (21, 25, 68). The first step of the PRX reaction cycle consists of the nucleophilic attack of the peroxidatic cysteine to one of the two oxygen atoms of H_2O_2 bound in the active site (26). The second-order rate constant of the nucleophilic substitution ($\text{S}_\text{N}2$) catalyzed by PRX with H_2O_2 (10^7 – $10^8 \text{ M}^{-1} \text{ s}^{-1}$) is typically six orders of magnitude higher compared with other proteins bearing H_2O_2 -sensitive cysteines with similar pK_a and similarly subjected to thiolate–sulfenic acid transitions (e.g., papain and protein tyrosine phosphatase 1B) (21). Clearly, the protein environment in which cysteines are located may play a crucial role by (i) increasing the nucleophilic character of the thiolate and/or (ii) increasing the electrophilic character of H_2O_2 . In both cases, the transition state of the $\text{S}_\text{N}2$ reaction is stabilized and the corresponding activation energy decreased (44).

Cysteine sulfenic acids formed in proteins upon reaction with H_2O_2 may undergo an electrophilic attack on a second thiol (either belonging to another cysteine molecule of the same protein or to reduced glutathione), resulting in a disulfide bond (Fig. 1), or launch a nucleophilic attack on another molecule of H_2O_2 to form sulfinic acid ($-\text{SO}_2\text{H}$) (Fig. 1). In a metabolically active cell compartment, such as the cytoplasm or the chloroplast stroma, thiols are easily

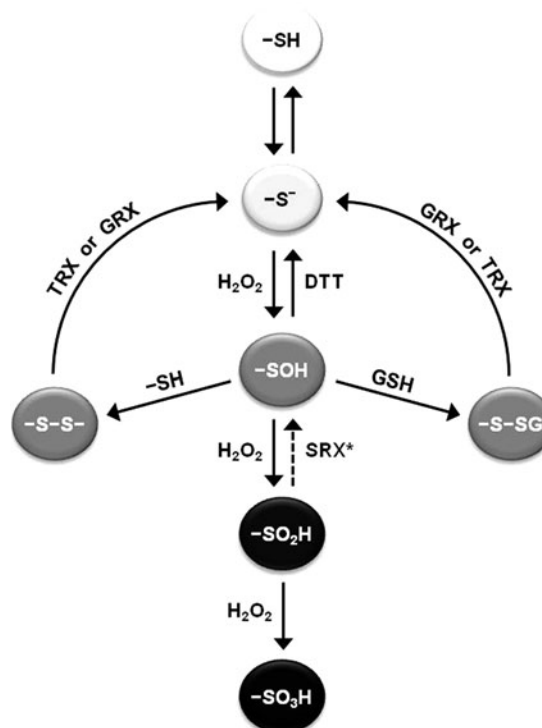


FIG. 1. Major reactions of protein cysteine sulfenic acids. Reactive cysteine thiols ($-\text{S}^-$) can undergo reversible oxidation to sulfenic acid ($-\text{SOH}$) in the presence of H_2O_2 . Subsequently, cysteine sulfenic acid can perform an electrophilic attack on a second thiol, either of another cysteine of the same protein or of glutathione resulting in a disulfide ($-\text{S}-\text{S}-$ or $-\text{S}-\text{SG}$, respectively), or nucleophilically react with two other molecules of H_2O_2 to sequentially form sulfinic and sulfonic acids ($-\text{SO}_2\text{H}$ and $-\text{SO}_3\text{H}$, respectively). Disulfides, but not sulfinates/sulfonates, can be reduced back by thioredoxins (TRXs) or glutaredoxins (GRXs). Only in the special case of peroxiredoxins, sulfinates are recovered to sulfenic acids by ATP-dependent sulfiredoxins (SRXs, as indicated by *). In all other proteins, sulfinates/sulfonates are considered irreversible states of oxidized cysteines.

regenerated from disulfides by several physiological systems, including thioredoxins (TRXs) and glutaredoxins (GRXs) (3, 64). Reactions based on sulfenic acids as electrophiles are thus reversible *in vivo* and often involved in regulatory processes (31, 47). By contrast, sulfenic acids are considered irreversible modifications of cysteines, such as sulfonic acids ($-\text{SO}_3\text{H}$) that can derive from the reaction of sulfinic acids with a third H_2O_2 molecule (Fig. 1), and usually proceed toward protein degradation (44, 47). Only in the special case of PRXs, sulfinic acids formed under hyperoxidizing conditions are recovered to sulfenic acids by ATP-dependent sulfiredoxins (SRXs) (Fig. 1) (29). The fate of any given protein targeted by H_2O_2 in plant cells (i.e., redox signaling or protein degradation) would thus depend on the protein microenvironment surrounding selected cysteines as long as it can modulate the reactivity of the sulfenic acid intermediate.

GAPDH is a long known target of H_2O_2 modification due to its moderately acidic catalytic cysteine (11, 46, 65), which is physiologically involved in the nucleophilic attack on the substrate glyceraldehyde-3-phosphate (HCO-R ; G3P) to

form a hemithioacetal intermediate ($-S-CHOH-R$) (39). GAPDH is a ubiquitous and often abundant enzyme and its catalytic cysteine was reported to undergo different types of redox modification, including primary oxidation to sulfenic acid, disulfide, sulfinic, or sulfonic acid (11, 45, 65). Plants contain two photosynthetic GAPDH isoforms (A_4 - and A_2B_2 -GAPDHs), localized in chloroplasts and involved in the Calvin–Benson cycle for CO_2 fixation in the light and cytoplasmic glycolytic isoforms (C_4 -GAPDHs) (57, 65). All these isoforms are tetramers showing a conserved overall structure, but with differences in coenzyme specificity and regulation. Both chloroplastic and cytoplasmic GAPDHs have been identified in redox proteomic studies aimed at identifying the primary targets of different types of thiol-based redox post-translational modifications in plants (5, 27, 40, 41, 62, 66, 67).

In this study, we present a comparative study on the effect of H_2O_2 on isoform 1 of C_4 - and A_4 -GAPDH of *Arabidopsis thaliana* (therein named glycolytic isoform 1 of *Arabidopsis* GAPDH [AtGAPC1] and photosynthetic isoform of *Arabidopsis* GAPDH [AtGAPA], respectively). Both proteins are inactivated by H_2O_2 due to the specific and exclusive oxidation of catalytic Cys149. However, while the sulfenic acid formed in the AtGAPC1 active site is rapidly oxidized to sulfinic acid, this reaction is slower in AtGAPA, in spite of the similar acidity of the corresponding catalytic cysteines. Determination of the 3D structure of AtGAPC1 allowed identifying the few residues that differentiate the active site of AtGAPC1 from that of AtGAPA (19). Starting from these crystallographic structures, the reaction between H_2O_2 and the catalytic cysteines could be investigated using a quantum mechanical (QM) approach to obtain a mechanistic insight of the different reactivity of the cysteines in the two GAPDH isoforms. In our opinion, this work exemplifies how subtle

differences in protein environment can tune the stability of sulfenic acid groups, a property that may have wide physiological implications given the pivotal role of sulfenic acids in redox signaling.

Results

Overall structure of cytoplasmic AtGAPC1 and comparison with chloroplastic AtGAPA

The crystal structure of AtGAPC1, solved at a resolution of 2.3 Å, comprises a homodimer comprising chains O and R, each one binding an nicotinamide adenine dinucleotide (NAD^+) molecule and two sulfate ions (Fig. 2A). The two independent subunits are almost identical with an rmsd (root mean square deviation) of 0.37 Å on 331 superimposed C_α atoms. The whole tetramer is generated by a two-fold crystallographic axis coincident with the molecular symmetry axis Q. In the center of the tetramer, a sulfate ion with an occupancy factor (q) of 0.5 is observed (Fig. 2A), while the other two are found on the surface of chain R (not shown).

Each AtGAPC1 subunit comprises two domains: a coenzyme-binding domain (residues 1–147 and 313–331) and a catalytic domain (residues 148–312) (Fig. 2B). The coenzyme-binding domain shows an α/β folding pattern typical of the Rossmann fold. The catalytic domain folds into a mixed β -sheet of seven strands and three α -helices and contains a long ordered loop, called S-loop, stretching from residue 177 to 203 (Fig. 2B). The S-loop contributes to the binding of the coenzyme, being in close proximity to its nicotinamide moiety and to the contact area between adjacent subunits (chains O/R; Fig. 2A).

A coenzyme NAD^+ is bound to each subunit in an extended conformation, stabilized by hydrogen bonds with protein

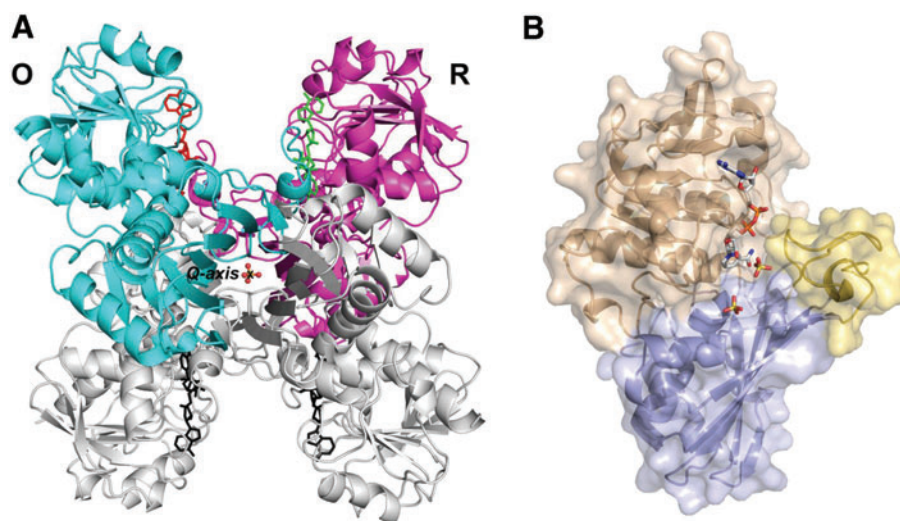


FIG. 2. Three-dimensional structure of AtGAPC1. (A) Cartoon representation of the AtGAPC1 tetramer. The crystallographic independent dimer OR is colored in cyan (chain O) and magenta (chain R), while the dimer generated by the twofold crystallographic axis is in gray. The nicotinamide adenine dinucleotide (NAD) molecules bound to each monomer are represented in stick; the sulfate ion observed at the center of the tetramer is shown in ball-and-stick representation. The symmetry molecular axis Q, coincident with a twofold crystallographic axis, is indicated. (B) Cartoon and surface representation of a single AtGAPC1 monomer. The domains are differently colored: cofactor-binding domain (wheat), catalytic domain (light blue), and S-loop (yellow). The bound NAD and sulfate ions are shown in stick representation. Atom colors: C light gray, N blue, O red, S yellow, and P orange. AtGAPC1, glycolytic isoform 1 of *Arabidopsis* GAPDH. To see this illustration in color, the reader is referred to the web version of this article at www.liebertpub.com/ars

residues and water molecules (Supplementary Fig. S1; Supplementary Data are available online at www.liebertpub.com/ars). The orientation of the nicotinamide ring is stabilized by an intramolecular hydrogen bond (NO1-NN7) and by a hydrophobic interaction with the side chain of Ile11, while a different orientation is sterically hindered by the side chain of Tyr311 (Supplementary Figs. S1, S2). On the other hand, the adenine ring is set in place by two phenylalanine residues (Phe37 and Phe99) and Thr96 (Supplementary Fig. S2). The aromatic ring of Phe37 is exactly perpendicular to the NAD⁺ adenine ring and it has been reported that this residue contributes to stabilize the NAD⁺ binding (56).

The active site of AtGAPC1 includes catalytic Cys149, whose thiol group lies between the side chain of His176, the second catalytic residue, and the nicotinamide ring of the cofactor (Fig. 3). Two sulfate ions from the crystallization medium occupy the sites P_S and P_I that accommodate the phosphate groups of the substrates during the catalysis (39). The sulfate located into the P_S site is closer to the coenzyme compared with the other one and interacts with the 2'-hydroxyl group of the nicotinamide ribose. Moreover, it is stabilized by a strong electrostatic interaction with Arg231 and is hydrogen bonded to Thr179, Thr181, and a water molecule (W49; Fig. 3). The P_I-sulfate ion forms hydrogen bonds with Ser148, Thr208, Gly209, and a water molecule (W181; Fig. 3).

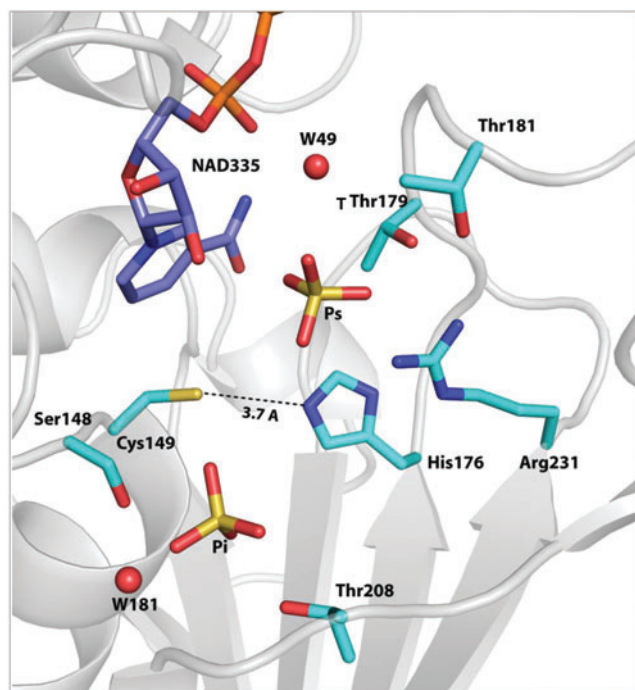


FIG. 3. Representation of the active site of AtGAPC1 monomer O. The distance between the thiol and the amino groups of the catalytic residues Cys149 and His176, respectively, is indicated. The NAD and the residues stabilizing the two sulfate ions occupying the P_S and the P_I sites are shown in stick representation and as spheres for water molecules. Atom colors: C cyan (GapC1 residues) and light blue (NAD), N blue, O red, S yellow, and P orange. To see this illustration in color, the reader is referred to the web version of this article at www.liebertpub.com/ars

The overall structure of AtGAPC1 is similar to archeal, bacterial, and eukaryotic GAPDHs (52, 65). In particular, it is almost identical to cytoplasmic GAPDH from *Oryza sativa*, the only other structure of plant cytoplasmic GAPDH currently available (56). The two enzymes share a sequence identity of 86% (Supplementary Fig. S3) and their C_α atoms can be superimposed with an rmsd of 0.62 Å. Some minor structural differences are observed between AtGAPC1 and a chloroplast GAPDH isoform of the same species (AtGAPA) (19). Sequence identity between AtGAPC1 and AtGAPA decreases to 46% (Supplementary Fig. S4) and tetramer superimposition shows a higher deviation (rmsd 1.34 Å; C_α atoms). Within subunits (rmsd 0.96 Å), cofactor-binding domains (rmsd 2.24 Å) are clearly more divergent than catalytic domains (rmsd 0.76 Å). The active site is quite well conserved, with the two catalytic residues (Cys149 and His176) located at similar distance in both proteins (3.7 Å in AtGAPC1, Figure 3; 3.4 Å in AtGAPA, Supplementary Fig. S5).

AtGAPC1 and AtGAPA contain a similarly acidic catalytic cysteine

The activity of GAPDH is based on the nucleophilic character of the catalytic Cys149 residue, which covalently binds the substrate (BPGA or G3P) during the catalytic cycle (65). The alkylating agent, iodoacetamide (IAM), specifically reacts with cysteine thiolates, and the alkylation of Cys149 inhibits GAPDH activity. Consistently, by assaying the residual activity of both AtGAPC1 and AtGAPA after IAM treatments at different pH values, a pH-dependent inhibition was observed (Supplementary Fig. S6A). The presence of BPGA during IAM incubation fully prevented the inactivation of both enzymes (Supplementary Fig. S6B), in agreement with the notion that IAM inactivates GAPDH through alkylation of catalytic Cys149.

Moreover, the capability of IAM to alkylate Cys149 thiolates allowed the determination of the ionization constant (pK_a) of Cys149. This analysis revealed that AtGAPA catalytic cysteine (pK_a 6.01 ± 0.04; Table 1 and Supplementary Fig. S6C) is slightly less acidic than its counterpart in AtGAPC1 (pK_a 5.65) (5), but still much more acidic than a free cysteine (44).

Catalytic Cys149 is the target of H₂O₂-dependent oxidation

In both AtGAPC1 and AtGAPA, treatments with H₂O₂ led to inhibition of enzyme activity (Figs. 4 and 5). Preincubation with BPGA fully protected from H₂O₂ inhibition (Fig. 4C), again suggesting that Cys149 was the target of the modification, but not excluding that other cysteines may also be modified.

AtGAPC1 sequence contains a total number of two cysteines, one at position 149 and one at position 153 (Fig. 4A). Both are highly conserved among GAPDHs of different species (22). AtGAPA has five cysteines, including Cys149 and Cys153 (Fig. 4A). Catalytic Cys149 is quite accessible to the solvent in both proteins, having a calculated accessible surface area (ASA) of 7.9 Å² in AtGAPC1 and 6.9 Å² in AtGAPA (Fig. 4B). On the contrary, Cys153 is deeply buried in a hydrophobic cavity (ASA equal to 0.0 in both GAPDHs) and its thiol group is ~9 Å away from the catalytic thiol,

TABLE 1. CYSTEINE ACIDITY AND H₂O₂ REACTIVITY OF AtGAPC1 AND AtGAPA

Protein	K_{RSH}	pK_a	ionized fraction at pH 7.0	K_{RS}^-
AtGAPC1	$54 M^{-1} s^{-1}$	$5.65^a \pm 0.03$	0.960	$56 M^{-1} s^{-1}$
AtGAPA	$31 M^{-1} s^{-1}$	6.01 ± 0.04	0.907	$34 M^{-1} s^{-1}$

^avalue from (5).

AtGAPA, photosynthetic isoform of Arabidopsis GAPDH; AtGAPC1, glycolytic isoform of Arabidopsis GAPDH (isoform 1).

making unfeasible the formation of a Cys149-Cys153 disulfide bond, as recently demonstrated for human GAPDH (45). The accessibility of the other three cysteines of AtGAPA varies from the very low value of Cys18 (ASA 1.7 Å²) to the high values of Cys274 (ASA 14.7 Å²) and Cys 285 (ASA 65.5 Å²) (Fig. 4B). The thiol groups of these three residues lie

between 13.5 and 19.8 Å from the catalytic thiol of Cys149, excluding direct interactions between these functional groups.

To test whether further cysteine residues were susceptible to oxidation, the number of free thiols was determined before and after H₂O₂ treatment (Fig. 4D). Consistent with structural data and solvent accessibility calculations, AtGAPAC1 had

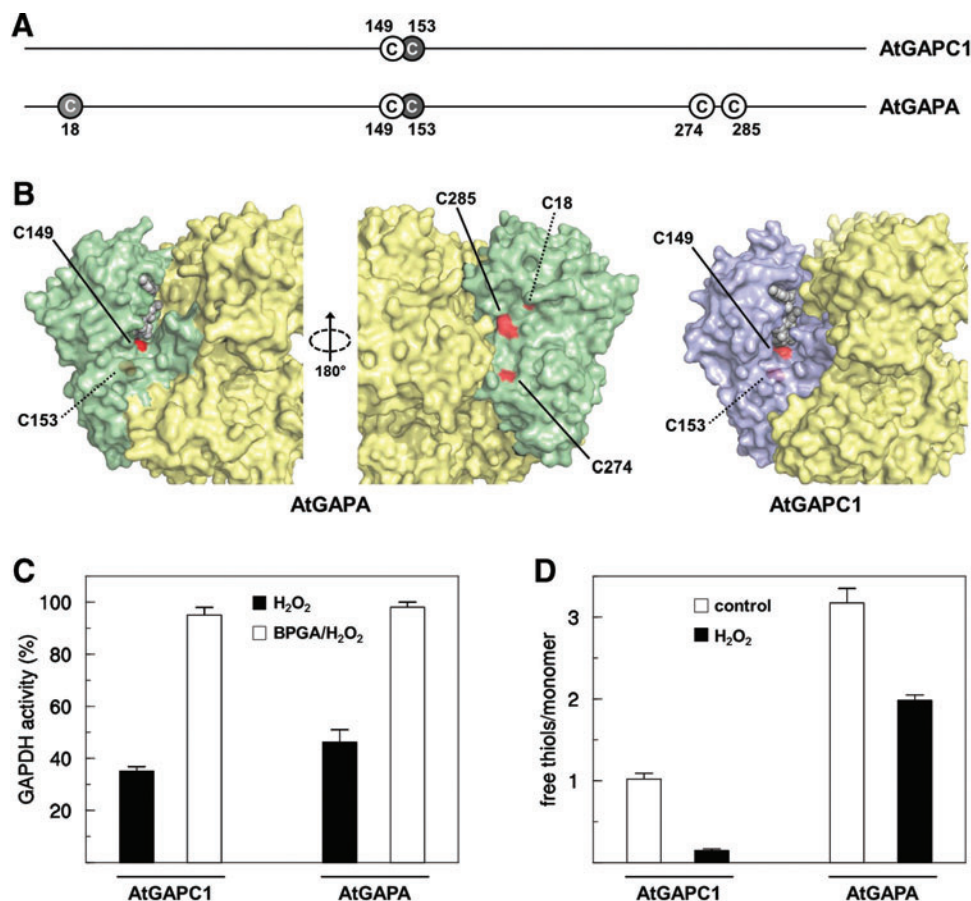


FIG. 4. Cysteine position, conservation, and accessibility in AtGAPC1 and AtGAPA, and sensitivity of catalytic Cys149 to H₂O₂-dependent oxidation. (A) Schematic representation of cysteine localization/conservation in AtGAPC1 and AtGAPA. Accessible cysteines are shown on a *white* background, while buried cysteines on a *gray* background. Cysteine residues are numbered according to the crystallographic structures (PDB codes: 4Z0H for AtGAPC1 and 3K2B for AtGAPA). (B) Surface representation of AtGAPA and AtGAPC1 structures, showing the position and the different accessibility of cysteine residues (highlighted in *red*). A single monomer is colored in *light green* for AtGAPA and *light blue* for AtGAPC1, while the other three subunits are shown in *yellow*. Two side views of AtGAPA tetramer differing by 180° are reported. (C) Inhibition and substrate protection of H₂O₂-dependent oxidation. Reduced proteins were incubated for 10 min with 50 μM H₂O₂ alone (*black bars*) or in the presence of the BPGA-generating system (3 mM 3-phosphoglycerate, 5 units/ml of 3-PGK, and 2 mM ATP) (*white bars*). After incubation, NAD(P)H-dependent activity was determined. Data are represented as the mean percentage of maximal control activity ± standard deviation (SD) (*n*=3). (D) Determination of cysteine thiols in AtGAPC1 and AtGAPA. The number of free cysteine thiols was determined by measuring TNB⁻ formation at 412 nm during incubation of untreated and H₂O₂-treated proteins with DTNB. Data represent the average (± SD) of two independent experiments. AtGAPA, photosynthetic isoform of Arabidopsis GAPDH. To see this illustration in color, the reader is referred to the web version of this article at www.liebertpub.com/ars

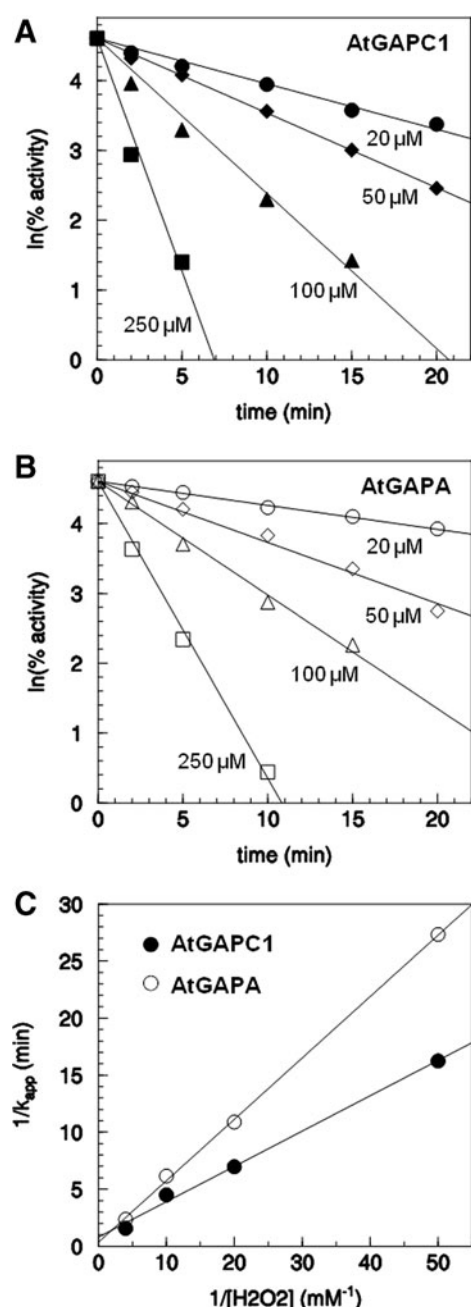


FIG. 5. Kinetics of inactivation of AtGAPC1 and AtGAPA. (A) Time- and concentration-dependent inactivation of AtGAPC1 by H₂O₂. From top to bottom: 20, 50, 100, and 250 μM H₂O₂. (B) Time- and concentration-dependent inactivation of AtGAPA by H₂O₂. From top to bottom: 20, 50, 100, and 250 μM H₂O₂. (C) Double-reciprocal plots of k_{app} versus H₂O₂ concentrations obtained according to Kitz and Wilson (30) to yield K_1 and k_{inact} (AtGAPC1, open circles; AtGAPA, closed circles). Each data point represents the mean of three independently obtained data sets. The straight lines represent the best-fit linear regression through the raw data.

one accessible thiol (1.02 ± 0.1), while three accessible thiols were detected in AtGAPA (3.2 ± 0.2). After treatment with H₂O₂, the number of free thiols decreased by one unit in both proteins (0.12 ± 0.05 in AtGAPC1 and 1.98 ± 0.3 in AtGAPA). Under present conditions, catalytic Cys149 is therefore

the only cysteine that can be modified by H₂O₂ in both AtGAPC1 and AtGAPA, and this is the reason for the H₂O₂-dependent enzyme inhibition.

Cytoplasmic AtGAPC1 is more sensitive to H₂O₂ oxidation than chloroplast AtGAPA

The oxidation rates of AtGAPC1 and AtGAPA were determined by incubating both proteins with varying concentrations of H₂O₂ (Fig. 5A, B). Using H₂O₂ in large excess with respect to enzyme concentration, the inactivation reaction obeyed pseudo first-order kinetics, and apparent first-order inactivation constants (k_{app}) could be determined at each H₂O₂ concentration. Second-order rate constants ($K'_{RS(H)}$) were derived from the slope of double reciprocal plots according to Kitz-Wilson (30) (Fig. 5C). These values were higher for AtGAPC1 ($54 \text{ M}^{-1} \text{ s}^{-1}$) than AtGAPA ($31 \text{ M}^{-1} \text{ s}^{-1}$) (Table 1). These rate constants refer to the reaction between total catalytic thiols and H₂O₂ at pH 7.0 and depend on the amount of catalytic cysteines that are deprotonated at the given pH. By taking into account the molar fraction of Cys149 thiolates at neutral pH (0.96 for AtGAPC1 and 0.91 for AtGAPA, Table 1), pH-independent rate constants (K_{RS^-}) could be derived (AtGAPC1: $56 \text{ M}^{-1} \text{ s}^{-1}$; AtGAPA: $34 \text{ M}^{-1} \text{ s}^{-1}$; Table 1). These are second-order rate constants for the reaction of thiolates with H₂O₂. Overall, these results indicate that sulfenic acid formation in the active site of AtGAPC1 proceeds faster than in AtGAPA, but this property of AtGAPC1 little depends on the acidity of its catalytic cysteine.

Cysteine sulfenic acids in the active site of AtGAPC1 react faster with H₂O₂ with respect to AtGAPA

The sulfenic acid formed in the active site of H₂O₂-treated GAPDH can be reduced back to its thiol form by a reducing agent such as dithiothreitol (DTT) (44). Sulfinate or sulfonate forms, possibly deriving from further oxidation of sulfenic acids by H₂O₂, do not react with DTT and are generally considered irreversible modifications (44, 47, 64). Therefore, after incubation with excess DTT, the amount of sulfenic acid formed by the reaction with H₂O₂ could be extrapolated from the recovery of enzyme activity (Fig. 6). In experiments with AtGAPC1 (2.5 μM), the highest level of sulfenic acid detected with this method was ~10% (after 10-min treatment with 20 μM H₂O₂) (Fig. 6A). Under these conditions, ~50% of the protein was still active ($-S^-$) and ~40% underwent irreversible oxidation ($-SO_nH$). At higher H₂O₂ concentrations, accumulation of sulfenic acid became negligible and AtGAPC1 was totally and irreversibly inactivated. Same treatment with 20 μM H₂O₂ applied to AtGAPA (2.5 μM) left ~70% of the protein in the active state ($-S^-$), while the remaining ~30% was in the sulfenic acid form (Fig. 6B). Irreversibly oxidized forms appeared in AtGAPA only with H₂O₂ concentrations higher than 20 μM (or longer incubation times). The reactivity of sulfenic acids with H₂O₂ generating further oxidized forms (*i.e.*, sulfenic/sulfonic acids) was clearly faster in AtGAPC1 than AtGAPA.

This conclusion was confirmed by incubating AtGAPC1 and AtGAPA with equimolar H₂O₂ concentrations for variable times (Fig. 7, Supplementary Table S1). After 30 min, ~5% of AtGAPC1 and ~30% of AtGAPA were in sulfenic acid form ($-SOH$). After 90 min, the reaction reached a plateau. Under these conditions, ~50% of AtGAPC1 was

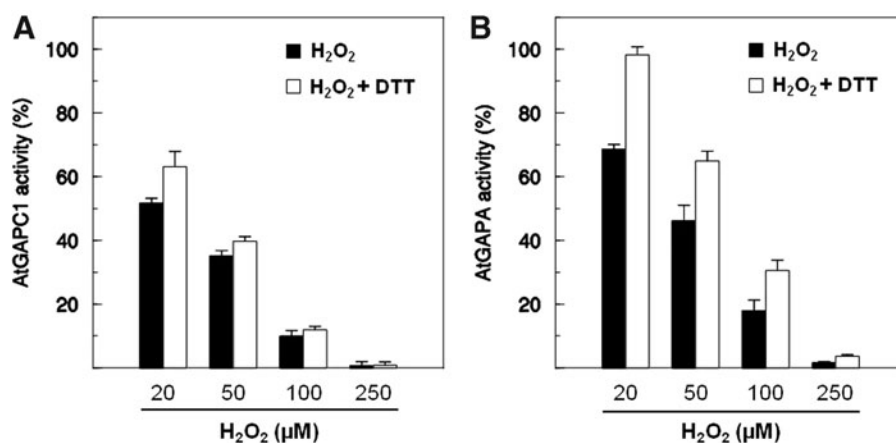


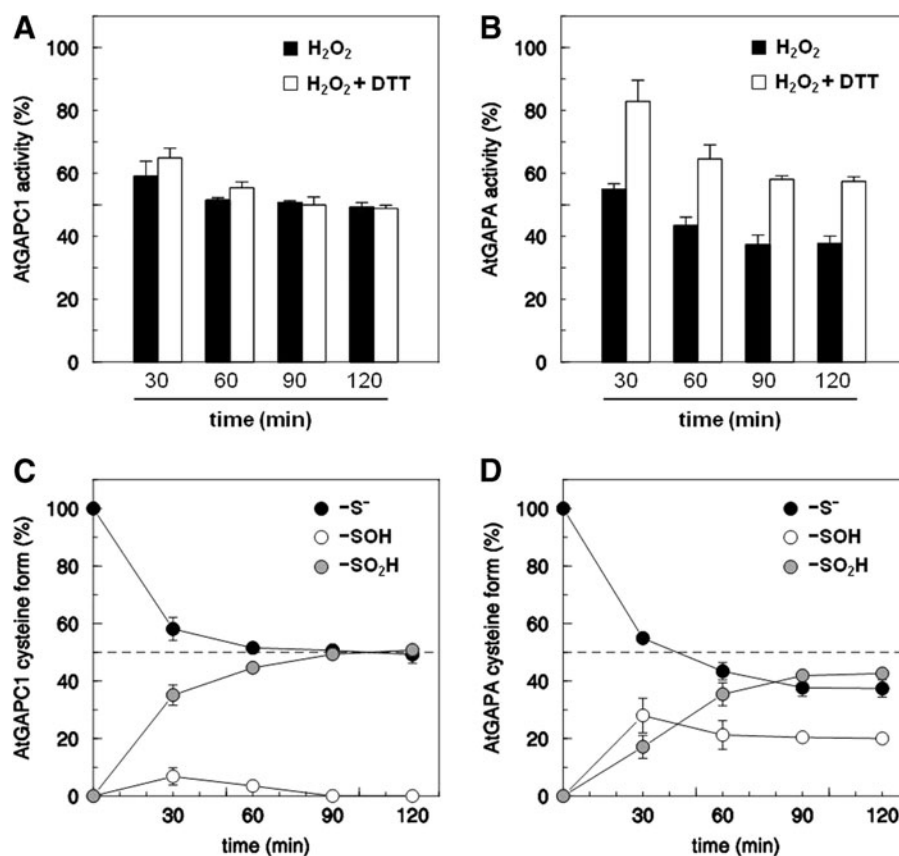
FIG. 6. Reversibility of H_2O_2 treatments. (A) Reduced AtGAPC1 was incubated for 10 min with H_2O_2 at different concentrations ranging from 20 to 250 μM (black bars). The reversibility of AtGAPC1 inactivation at each H_2O_2 concentration was assessed by incubation for 10 min in the presence of 20 mM dithiothreitol (DTT) (white bars). NADH-dependent glyceraldehyde-3-phosphate dehydrogenase (GAPDH) activity was then determined. (B) Reduced AtGAPA was incubated for 10 min with H_2O_2 at different concentrations ranging from 20 to 250 μM (black bars). The reversibility of AtGAPA inactivation at each H_2O_2 concentration was assessed by incubation for 10 min in the presence of 20 mM DTT (white bars). NADPH-dependent GAPDH activity was then determined. For both panels, data are represented as the mean percentage of maximal control activity \pm SD ($n=3$).

irreversibly inactivated, while $\sim 50\%$ was still active ($-S^-$) (Fig. 7A, C, and Supplementary Table S1); AtGAPA was instead $\sim 40\%$ active ($-S^-$), $\sim 20\%$ DTT recoverable ($-SOH$), and $\sim 40\%$ irreversibly oxidized ($-SO_2H$) (Fig. 7B, D, and Supplementary Table S1), confirming once again that the sulfenic acid was more stable in the catalytic site of AtGAPA than in AtGAPC1.

No evidence of cysteinyl sulfonate formation in GAPDH active sites

The irreversible inactivation of 50% AtGAPC1 in the presence of equimolar H_2O_2 was compatible with a two-step oxidation of Cys149 to the sulfinate form. Whether AtGAPC1-sulfinate could undergo further oxidation to

FIG. 7. Incubation of AtGAPC1 and AtGAPA with equimolar concentration of H_2O_2 . AtGAPC1 (A) and AtGAPA (B) were incubated in the presence of equimolar concentration of H_2O_2 . At the indicated time, aliquots were withdrawn from the incubation mixtures and assayed for NAD(P)H-dependent GAPDH activity before and after incubation with DTT. The activity percentages of active/reduced ($-S^-$), inactive/reactivated ($-SOH$), and irreversibly inactivated ($-SO_2H$) for AtGAPC1 and AtGAPA are represented in (C, D), respectively. Data represented in (C, D) are listed in Supplementary Table S1. For all panels, data are represented as the mean percentage of maximal control activity \pm SD ($n=3$).



sulfonate was tested after full and irreversible inactivation of 10 μM AtGAPC1 with 50 μM H_2O_2 . Residual H_2O_2 concentration determined by Amplex[®] Red at the end of the reaction was $30.2 \pm 1.3 \mu\text{M}$, demonstrating that two equivalents of H_2O_2 ($\sim 20 \mu\text{M}$) reacted twice with one equivalent of AtGAPC1 ($\sim 10 \mu\text{M}$), giving rise to 10 μM sulfinate forms. Even with H_2O_2 in excess, AtGAPC1 oxidation ended up with sulfinate forms with no evidence of sulfonate formation at significant rates. Identical experiments performed with AtGAPA gave rise to the same conclusion. After complete and irreversible inactivation of 10 μM AtGAPA, only $19.4 \pm 0.1 \mu\text{M}$ H_2O_2 was consumed in the reaction, consistent with the conversion of Cys149 to the sulfinic form.

Potential energy surfaces for the oxidation of thiolate to sulfonic acid as calculated by quantum mechanics of Arabidopsis GAPDH active sites

Biochemical evidence has demonstrated that the oxidation of catalytic Cys149 by H_2O_2 occurs at different rates in AtGAPC1 versus AtGAPA. As a consequence, the sulfinic acid shows different persistency in the two protein environments. To elucidate the mechanistic aspect, QM calculations, based on the crystallographic structures of AtGAPC1 (this work) and AtGAPA (19), were carried out to investigate the reaction potential energy surface (PES) for the three-step oxidation of Cys149 by H_2O_2 . The effect of the different protein environments on the whole oxidation process could then be assessed.

The starting model system for the QM investigation included all amino acids composed within a sphere with a radius of 8 Å, centered on the sulfur atom of catalytic Cys149 (Supplementary Fig. S7). Since all these amino acids were identical in both AtGAPC1 and AtGAPA, it was possible to describe the general thermodynamic parameters of cysteine oxidation in the core catalytic site of both proteins. The computed reaction energy profiles for the three consecutive oxidation steps, (1) thiolate to sulfinic; (2) sulfinic to sulfinic

acid; and (3) sulfinic to sulfonic acid, are reported in the three diagrams of Figure 8. Even if the three oxidation steps are highly exergonic and therefore irreversible, they are under kinetic control and the activation energies were predicted to grow significantly with the increase of the substrate oxidation state (Fig. 8).

These results suggested that sulfinic acid formation must proceed faster than sulfinic acid formation, allowing sulfinic acid to accumulate to some extent. Moreover, although sulfonic acid is the thermodynamically favored end product of the whole reaction, the high energy barrier of the last oxidation step (28 kcal mol^{-1}) suggested that sulfonic acid would not form at the temperature normally experienced by biological systems. This prediction is in full agreement with our Amplex Red determinations of residual H_2O_2 , showing that each catalytic cysteine of AtGAPA/AtGAPC1 can reduce no more than two molecules of H_2O_2 even after prolonged incubations. Based on these considerations, the oxidation of sulfinic to sulfonic acid was not further investigated.

Ping-pong proton transfer by the His176-Cys149 dyad

The reactivity toward H_2O_2 of any cysteine depends on both its acidity and nucleophilicity (21). In the case of GAPDHs, either AtGAPA or AtGAPC1, the acidity and nucleophilicity of Cys149 are tuned by His176, via a ping-pong proton transfer. QM computations on the model system, which represents the core catalytic site of both proteins, showed that the most stable structure of the His176-Cys149 dyad is a histidinium–thiolate ion pair (Supplementary Table S2 and Supplementary Fig. S8). In the presence of H_2O_2 , after the first oxidation step, the proton is transferred to the sulfinic acid and the neutral pair Cys149-OH-His176 is obtained. According to the hard and soft acid and base theory, the hard proton prefers to bind to the hardest basic site, that is, the negatively charged oxygen of cysteine Cys149-O[−] instead of the neutral soft nitrogen of the His176. For similar reasons, when the negative charge is delocalized on two or

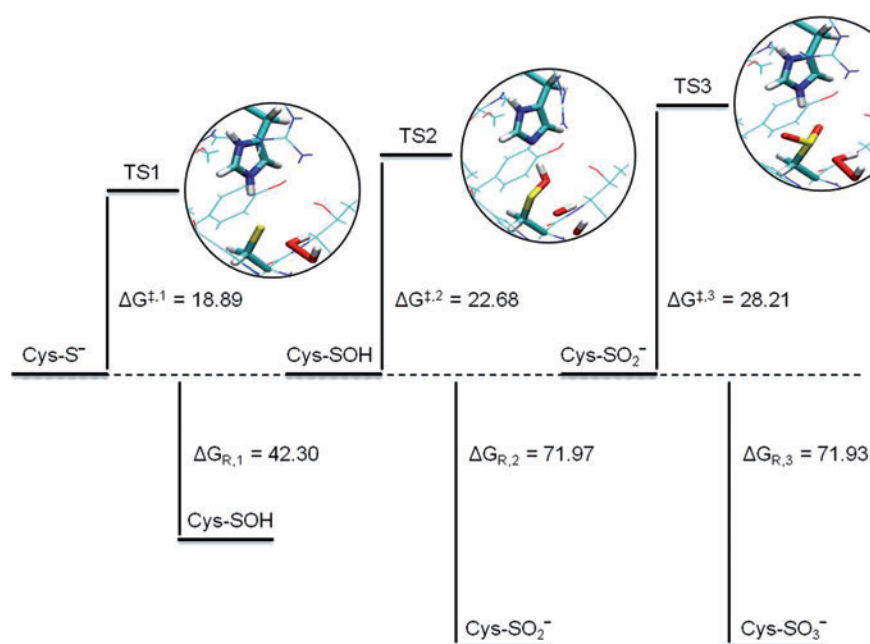


FIG. 8. Potential energy surface (PES) for the oxidation process of AtGAPDH active site. PES for the three-step process of oxidation from thiolate ($-\text{S}^-$) to sulfonic acid ($-\text{SO}_3\text{H}$) as calculated by quantum mechanical (QM). The model system for the QM investigation consisted of the core catalytic site of both AtGAPC1 and AtGAPA (Supplementary Fig. S7). Activation barrier and reaction-free energies (ΔG^\ddagger and ΔG_R , respectively) are expressed in kcal mol^{-1} . In the rounds, a blow-up of the transition states (TS1-TS3). To see this illustration in color, the reader is referred to the web version of this article at www.liebertpub.com/ars

three oxygen atoms as occurring in the sulfinic or sulfonic form of the cysteine, the proton prefers to bind to His176, forming again a salt bridge. Therefore, sulfenic acid is predicted to be the only protonated intermediate in the multistep oxidation of Cys149.

Fingerprint analysis identifies two arginines as the major factors responsible for the relative stability of sulfenic acid in AtGAPA

To get a deeper understanding of the results of biochemical analyses (showing that sulfenic and sulfinic acids are formed more rapidly in AtGAPC1 than in AtGAPA, Figs. 5–7), the energetic profile of the reaction between H_2O_2 and Cys149 was recalculated in the specific protein environment of either AtGAPC1 or AtGAPA. To emulate the different environments, we considered a larger sphere with a radius of 15 Å centered again on the sulfur atom of the catalytic Cys149 (Fig. 9). Within this sphere, the difference between AtGAPC1 and AtGAPA could be ascribed to 10 amino acids (Fig. 9). All these 10 amino acids were explicitly taken into account at a QM/molecular mechanical (MM) level by estimating the perturbation caused by each of them (MM charges) to the QM system (Fig. 10). With this approach, reaction energetic profiles could be recalculated for AtGAPC1 versus AtGAPA catalytic environments, and the effect of single amino acid substitutions could be enucleated by fingerprint analysis (Fig. 10) (14, 54, 55). Activation energies for both the first and second oxidation steps ($-\text{SOH}$ and $-\text{SO}_2\text{H}$ formation, respectively) were lower in AtGAPC1 (18.8 and 22.3 kcal mol $^{-1}$, respectively) than in AtGAPA (20.2 and 24.3 kcal mol $^{-1}$; Fig. 10, inset; Supplementary Table S3), in agreement with the observation that AtGAPC1 reacts faster with H_2O_2 than AtGAPA (Figs. 5–7).

The relative contribution of each specific amino acid to activation barriers was quantified by fingerprint analysis and two arginines of AtGAPA (Arg195 and Arg284, substituted by Gly195 and Val284 in AtGAPC1) were found to be the major factors responsible for the slower reactivity of AtGAPA-Cys149 in both oxidation steps (Fig. 10). In the formation of sulfenic acid, this effect was partially counterbalanced by Asp181 (substituted by Thr181 in AtGAPC1). Interestingly, neither of these amino acids occurs at an interaction distance <4 Å from the sulfur atom of Cys149.

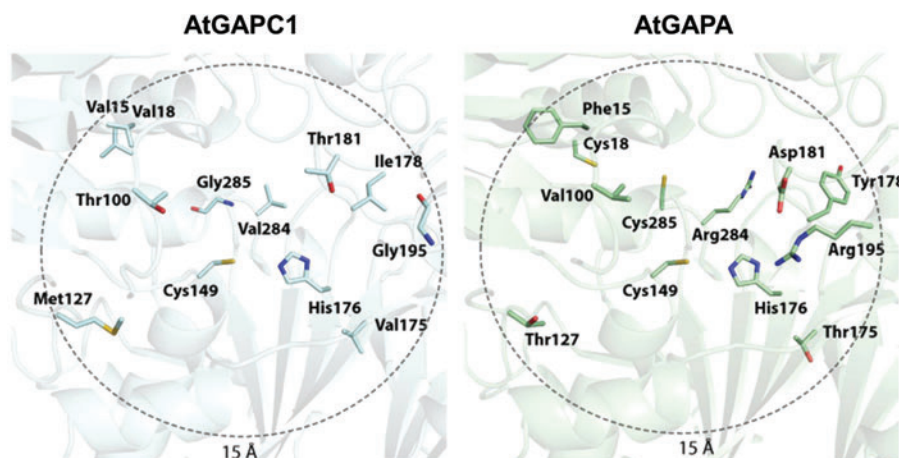
These data underpin the importance of electrostatic and polar interactions, even at long distance, provided by native protein environments in tuning cysteine reactivity (21). In the case of Arabidopsis GAPDHs, these effects prolong the lifetime of sulfenic acid in AtGAPA while promoting the irreversible oxidation of AtGAPC1 to sulfinic acid.

Discussion

Protein cysteine thiolates are much better nucleophiles than thiol groups and display higher propensity to H_2O_2 -dependent oxidation. At physiological pH values, the reaction of free cysteine thiolates with H_2O_2 ($26 \text{ M}^{-1}\text{s}^{-1}$) (21) is prevented by the high pK_a of the cysteine (8.6) (21, 31), and a similar situation holds true for glutathione (61, 64). On the other hand, several proteins react at physiological pH with H_2O_2 at significant rates, thanks to the acidity of their catalytic cysteines (21, 44). The pH-independent, second-order rate constant of these H_2O_2 -reacting cysteines is in the same order of free cysteine ($10\text{--}100 \text{ M}^{-1}\text{s}^{-1}$), but their actual reactivity *in vivo* is much higher because of their extensive deprotonation at physiological pH. Cysteine acidity depends on the microenvironment and although strong acidity correlates with decreased nucleophilicity of the thiolate (*i.e.*, less reactivity) (21), some proteins contain acidic cysteines (pK_a 4–6) that are largely deprotonated at physiological pH and still react with H_2O_2 at rates that can be compared with that of the free cysteine thiolate. As also shown in the current study, plant GAPDHs display these general properties.

The catalytic activity of GAPDH, consisting of the NAD(P)^+ -dependent oxidation of glyceraldehyde-3-phosphate (G3P, glycolytic reaction) or NAD(P)H -dependent reduction of 1,3-bisphosphoglycerate (BPGA, photosynthetic reaction), depends on Cys149. In the catalytic cycle of GAPDH, the sulfur atom of Cys149 performs a nucleophilic attack on the carbon atom of the substrate carbonyl, forming a covalent intermediate that is then converted into products. The reactivity of Cys149 is favored by moderate acidity, and in all GAPDHs, this is achieved *via* an interaction with His176 (this work; 65). Similar to many other enzymes bearing a catalytic cysteine (21), Cys149 and His176 form a dyad, in which the proton is shared between the sulfur atom of the cysteine residue and the $\text{N}_{\epsilon 1}$ of the imidazole ring. More precisely, in the GAPDH isoforms studied here, the shared proton is preferentially bound

FIG. 9. Amino acid differences between AtGAPC1 (left) and AtGAPA (right) considering a sphere of 15 Å centered on the sulfur atom of Cys149. The residues that are different between the two enzymes are shown in stick representation. Atom colors: *light cyan* (AtGAPC1) and *light green* (AtGAPA), *blue* (N), *red* (O), and *yellow* (S). To see this illustration in color, the reader is referred to the web version of this article at www.liebertpub.com/ars



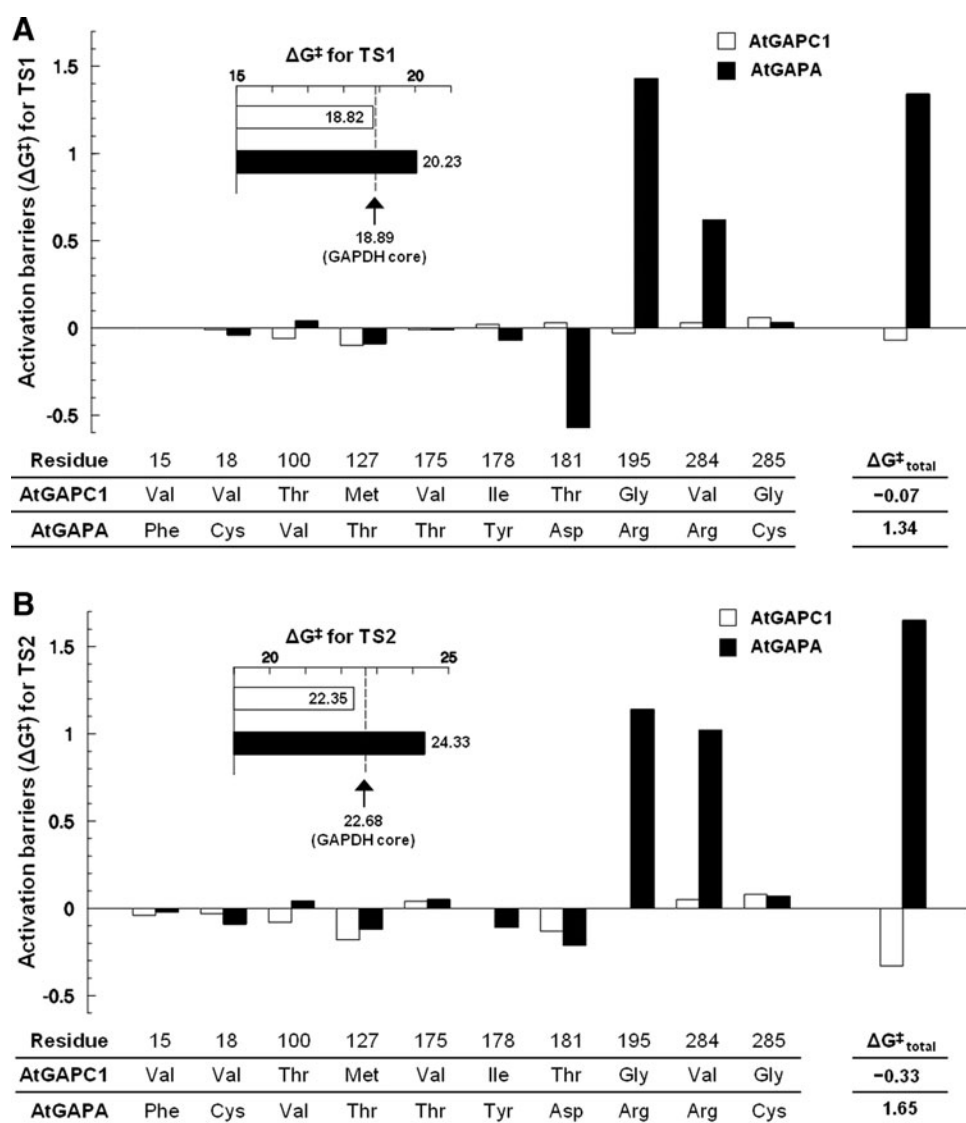


FIG. 10. Stabilizing/De-stabilizing effect of single amino acids in AtGAPC1 and AtGAPA on activation barriers for the two oxidation steps. (A) Stabilizing/De-stabilizing effect of single amino acids in AtGAPC1 and AtGAPA on activation barriers (ΔG^\ddagger , kcal mol⁻¹) for the transition state 1 (TS1, thiolate to sulfenic acid). *Inset*, activation barriers for TS1 of the core catalytic site of both enzymes (18.89 kcal mol⁻¹, indicated by a dashed line), of AtGAPC1 (18.82 kcal mol⁻¹, white bar), and of AtGAPA (20.23 kcal mol⁻¹, black bar) (B) Stabilizing/De-stabilizing effect of single amino acids in AtGAPC1 and AtGAPA on activation barriers for the transition state 2 (TS2, sulfenic to sulfinic acid). *Inset*, activation barriers for TS2 of the core catalytic site of both enzymes (22.68 kcal mol⁻¹, indicated by a dashed line), of AtGAPC1 (22.35 kcal mol⁻¹, white bar), and of AtGAPA (24.33 kcal mol⁻¹, black bar). For both panels, data are listed in Supplementary Table S3.

to the nitrogen atom: in this way, Cys149 is deprotonated and ready to perform the nucleophilic attack on the substrate (G3P or BPGA) or an alternative electron acceptor such as H₂O₂. Indeed, cytosolic AtGAPC1 and chloroplastic AtGAPA are both sensitive to H₂O₂-dependent inactivation. Experiments of BPGA protection coupled to thiol titration unequivocally demonstrated that in both proteins, Cys149 was the only target of H₂O₂ oxidation. Inhibition of enzyme activity was thus a consequence of Cys149 oxidation and no other cysteines were implied.

Crystallographic data showed that the core active sites of glycolytic AtGAPC1 (this work) and photosynthetic AtGAPA (19) are identical. This made it possible to build up a model system emulating the active site of both enzymes. This model system was used to compute at the QM level the energy profile of the reaction between Cys149 and H₂O₂ within a typical GAPDH active site. We found that all steps of cysteine oxidation (from thiolate to sulfonic acid) are highly exergonic; also, that energy barriers increased constantly from the first to the last oxidation step. Because of the arduous energetic barrier, sulfonic acid formation was actually

predicted to be unlikely at ambient temperature. Consistent with the model, we found no biochemical evidence of sulfonic acid formation in either AtGAPC1 or AtGAPA, suggesting that sulfinic acid could be the last oxidation state of catalytic Cys149 upon reaction with H₂O₂.

On the other hand, the prediction that in GAPDH active sites the conversion of the thiolate to sulfenic acid is faster than the subsequent conversion of sulfenic to sulfinic acid implies that sulfenic acids could accumulate to some extent. This property may have physiological relevance as long as the sulfenic acid might be involved in redox signaling events and, both AtGAPC1 and AtGAPA may undergo glutathionylation, which is a reversible type of modification (5, 66). However, in spite of their overall similarity, AtGAPC1 and AtGAPA showed, to some extent, a different reactivity toward H₂O₂, thus providing a clue to understand how sulfenic acids are differently stabilized in protein active sites.

Experimentally, we observed that AtGAPC1 reacts faster with H₂O₂ than AtGAPA and that sulfenic acids last longer in AtGAPA than in AtGAPC1. The QM investigation (based

on the high-resolution structures of both AtGAPA and AtGAPC1) showed that two arginine residues (Arg195 and Arg284) located at more than 8 Å (and <15 Å) from Cys149 in AtGAPA are the major factors responsible for this different behavior. Although these arginines do not interact directly with the Cys149-His176 dyad or with H₂O₂, their net positive charges possibly stabilize the negatively charged thiolate, thereby depressing its nucleophilic nature. Consistently, the negative carboxylate group of Asp181 partially counteracts this effect. This complex interplay of polarization and electrostatic effects determines the higher energetic barriers that characterize the single oxidation steps in AtGAPA. In general agreement with our calculations, a recent modeling of the oxidation pathway of methanethiol (CH₃SH) by H₂O₂ underlined the effect of polar molecules such as H₂O and NH₃ on reaction barriers (58).

Thus, long-range polarization effects explain why AtGAPC1 is more reactive toward H₂O₂ than AtGAPA and why the consecutive nucleophilic attack performed by Cys149-SOH on a second H₂O₂ is slower in AtGAPA than AtGAPC1. Interestingly, the relative stability of Cys149-SOH in AtGAPA has recently received an experimental confirmation by a proteomic study that identified AtGAPA, but not AtGAPC1, among 226 sulfenylated proteins in H₂O₂-stressed *Arabidopsis* cells (1). In spite of the lower stability of its sulfenic acid, AtGAPC1 is nevertheless a prominent target of H₂O₂ oxidation in these cells (59).

The protection of AtGAPA catalytic cysteine from detrimental overoxidation seems consistent with its localization in chloroplasts. As a consequence of oxygenic photosynthesis, chloroplasts are in fact the major source of ROS in green cells (23) and stromal proteins such as AtGAPA are an easy target for H₂O₂ produced by malfunctioning thylakoid complexes under photo-oxidative stress (41). Few amino acid substitutions are sufficient to make chloroplast AtGAPA more protected against overoxidation than cytoplasmic AtGAPC1. Thanks to its long-lasting sulfenic acid, AtGAPA might be more easily glutathionylated and its activity rescued by the chloroplast glutathione/GRX system (64).

On top of that, chloroplasts contain a regulatory protein named CP12 that under specific conditions can assemble a supramolecular complex, in which AtGAPA is shielded from H₂O₂ (16, 20, 35), again suggesting that redox-sensitive proteins of chloroplasts need effective protection mechanisms against oxidative stress. Not only AtGAPA but also all enzymes of the Calvin–Benson cycle that are essential for photosynthetic growth can be glutathionylated and possibly protected by this post-translational modification (37). On the other hand, cytoplasmic AtGAPC1 is more vulnerable to overoxidation than its chloroplast counterpart. The cytoplasm probably experiences lower levels of oxidative stress than actively photosynthesizing chloroplasts, but nevertheless the prompt oxidation of AtGAPC1 may be meaningful *in vivo* (59). Recent evidence clearly demonstrated that oxidation of human GAPDH is a key component of the cellular adaptive responses to increased H₂O₂ levels. Experimental data supported the view that GAPDH inactivation has the effect of rerouting the glycolytic flux toward the pentose phosphate pathway, thereby favoring the regeneration of the NADPH required to recover reversibly oxidized proteins *via* TRXs and glutaredoxins (45). In plants, a similar adaptive response based on cytosolic

GAPDH sensitivity to H₂O₂ appears very likely, although not yet demonstrated (28, 46, 65).

In conclusion, we have shown here how the protein environment can affect both the reactivity of a cysteine with H₂O₂ and the stability of the resulting sulfenic acid. This property is relevant for redox signaling mechanisms that are largely based on the capacity of cysteine sulfenic acids to avoid overoxidation and, in turn, progress toward reversible modifications such as glutathionylation.

Materials and Methods

Materials and enzymes

NAP-5 columns were obtained from GE Healthcare (Piscataway, NJ). H₂O₂ was purchased from Sigma-Aldrich (St. Louis, MO) and quantified spectrophotometrically using a molar extinction coefficient at 240 nm of 43.6 M⁻¹ cm⁻¹. The Amplex Red (10-acetyl-3,7-dihydroxyphenoxazine) H₂O₂/peroxidase assay kit was purchased from Life Technologies (Carlsband, CA). All other chemicals were obtained from Sigma-Aldrich unless otherwise specified. Phosphoglycerate kinase (PGK) from *S. cerevisiae* was purchased from Sigma-Aldrich. Recombinant GAPC1 and GAPA from *Arabidopsis thaliana* (AtGAPC1 and AtGAPA, respectively) were expressed and purified according to (5, 36, 53). The molecular mass and purity of the proteins were analyzed by SDS-PAGE after dialysis against 50 mM potassium phosphate (pH 7.5). The concentration of purified AtGAPC1 and AtGAPA was determined spectrophotometrically using a molar extinction coefficient at 280 nm of 40910 M⁻¹ cm⁻¹ and 36250 M⁻¹ cm⁻¹, respectively.

Activity assay

AtGAPC1 and AtGAPA activities were monitored spectrophotometrically at 340 nm and 25°C by following the oxidation of NAD(P)H in an assay mixture containing 50 mM Tris-HCl, pH 7.5, 1 mM EDTA, 5 mM MgCl₂, 3 mM 3-phosphoglycerate, 5 units ml⁻¹ of baker's yeast PGK, 2 mM ATP, and 0.2 mM NADH (AtGAPC1 assay) or 0.2 mM NADPH (AtGAPA assay).

Alkylating treatments and determination of the pK_a of the catalytic cysteine of AtGAPA

Before any treatments, AtGAPC1 and AtGAPA were reduced with 10 mM reduced DTT for 1 h at room temperature. DTT was subsequently removed by desalting on NAP-5 columns equilibrated with 50 mM Bis-Tris, pH 7.0. Reduced AtGAPC1 and AtGAPA (2 μM) were incubated in 50 mM sodium citrate (pH 5.0) or in 50 mM Bis-Tris (pH 7.0) or in 50 mM glycine (pH 9.0) in the presence of 0.2 mM IAM. All reaction mixtures contained 0.14 mM NAD⁺. After 10 min of incubation, aliquots were withdrawn for the assay of enzyme activity. Substrate protection was performed by pre-incubating (5 min) the proteins in the presence of a BPGA (1,3-bisphosphoglycerate)-generating system (3 mM 3-phosphoglycerate, 5 units/ml of 3-PGK and 2 mM ATP). The pH dependence of the inactivation of AtGAPA by IAM was carried out by following a procedure described in a previous study (5). Briefly, the reduced protein (2 μM) was incubated with or without IAM (0.2 mM) for 20 min in different buffers with a pH range from 3 to 10. After incubation, AtGAPA

activity was determined. The residual activity expressed as a percentage of maximal activity was plotted versus pH, and the ionization constant (pK_a) was calculated by fitting the experimental data to a derivation of the Henderson–Hasselbalch equation as previously described (63).

Inactivation of AtGAPC1 and AtGAPA by H₂O₂

Reduced AtGAPC1 and AtGAPA (2.5 μ M or otherwise indicated) were incubated in 50 mM Bis-Tris buffer (pH 7.0) supplemented with 0.14 mM NAD⁺ in the presence of H₂O₂ at the indicated concentrations. Substrate protection was performed by preincubating (5 min) the proteins in the presence of a BPGA (1,3-bisphosphoglycerate)-generating system (3 mM 3-phosphoglycerate, 5 units/ml of 3-PGK and 2 mM ATP). At different times, aliquots were withdrawn from the incubation mixture and assayed for enzyme activity. All inactivation experiments were monitored relative to a control sample without H₂O₂, which was set to 100% activity at each time point. Kinetic parameters of H₂O₂ inhibition for AtGAPC1 and AtGAPA were determined according to the Kitz–Wilson plot (30). The reversibility of protein inactivation by H₂O₂ was assessed by measuring GAPDH activities after 10 min of incubation of H₂O₂-treated proteins in the presence of 20 mM DTT.

Quantification of H₂O₂ by amplex red

AtGAPC1 and AtGAPA were treated with a fivefold molar excess of H₂O₂ until no protein activity was detected prior and after DTT treatment. The residual H₂O₂ was then quantified by Amplex Red/horseradish peroxidase (AR/HRP) assay, following the manufacturer's instruction. Briefly, protein samples were diluted twofold in 50 mM Bis-Tris buffer and incubated with 50 μ M AR in the presence of 1 U/ml HRP. After 10 min of incubation, the absorbance at 570 nm was measured by using a plate reader (Victor³ Multilabeling Counter; Perkin Elmer, Waltham, MA). Because the determination of H₂O₂ by the AR/HRP method is not direct, the amount of H₂O₂ in the samples was determined by constructing standard curves using known H₂O₂ concentrations in the range 2.5–40 μ M. Samples containing AtGAPC1 or AtGAPA without H₂O₂ were used as blanks.

Determination of free thiol groups

AtGAPC1 and AtGAPA were treated as described above. The excess of H₂O₂ was removed by desalting on NAP-5 columns equilibrated with 50 mM Tris-HCl buffer (pH 7.9). The number of free thiols of untreated and H₂O₂-treated proteins was then determined spectrophotometrically with DTNB, as previously described (6).

Replicates

All the results reported are representative of at least three independent experiments and expressed as mean \pm standard deviation.

Crystallization and data collection

Purified AtGAPC1 was concentrated to 10 mg ml⁻¹ in 50 mM potassium phosphate (pH 7.5) containing 1 mM

NAD⁺ and crystallized by the hanging drop vapor diffusion method at 293 K. The drop, formed by a protein solution aliquot of 2 μ l mixed with an equal volume of reservoir, was equilibrated against 750 μ l of reservoir.

Rhombohedral crystals grew after about 3 weeks from a solution containing 3.0–3.5 M ammonium sulfate and 0.1 M Hepes-NaOH, pH ranging between 7.5 and 8.5. Prismatic crystals were obtained from 18% w/v PEG 4K and 0.1 M Na-acetate pH 4.6. Crystals were fished from the crystallization drop, briefly soaked in a cryo solution containing 3.5 M ammonium sulfate and 10% v/v glycerol for the first crystal form, or 20% w/v PEG 4K and 10% v/v PEG 200 for the second one, and then frozen in liquid nitrogen. Data collections were performed at ESRF (beam line ID14-4) at 100 K using a wavelength of 0.939 Å and an ADSC Quantum Q315r detector. The images were indexed and integrated by iMosflm (4) and scaled with POINTLESS and SCALA from the CCP4 package (18). The diffraction data confirmed that the two crystal forms correspond to different polymorphs. Crystals grew using ammonium sulfate as precipitant, indicated as polymorph 1, and diffracted to a better resolution with respect to crystals indicated as polymorph 2. Data collection statistics are reported in Supplementary Table S4.

Structure solution and refinement

The structure of polymorph 1 was solved by molecular replacement using the software from the program suite IL MILIONE (10). The coordinates of AtGAPA (PDB code: 3K2B) (19), deprived of the cofactor and water molecules, were used as a search model. The correctness of the solution was verified by building the whole crystal packing. The refinement was performed by CNS1.3 (9), selecting 5% of reflections for R_{free}, and the manual rebuilding by Coot (17). NAD⁺ and sulfate ions were inserted after few refinement cycles in the electron density regions not occupied by the protein chains. In the final stages of refinement, water molecules were automatically added, and after a visual inspection, they were conserved in the model only if contoured at 1.0 σ on the (2F_o–F_c) map and if they fell into an appropriate hydrogen bonding environment. Stereochemical quality of the models was checked with PROCHECK (33). The Ramachandran plots show that 98.6% of residues lie in the most favored plus additional allowed regions. Only 0.7% of residues are found in disallowed regions. Refinement statistics are reported in Supplementary Table S4.

Accession number

The atomic coordinates and structure factors of AtGAPC1 structure have been deposited in the Protein Data Bank with the accession code 4Z0H.

Computational details

The crystallographic structures of AtGAPC1 (this work) and AtGAPA (19), to which we manually added the H₂O₂ molecule, were used as the starting point. The hydrogen atoms were included at pH 7.4 using the H++ online program (2).

Choice of the residues

The choice of a suitable model system is crucial in the investigation of enzyme mechanisms and it must primarily include all groups that are supposed to play a key role in the reaction. Thus, to examine in detail the oxidation of Cys149 by H_2O_2 , we built a model system, including all amino acids or cofactors within a sphere with a radius of 8 Å centered on the sulfur atom of catalytic Cys149 (Supplementary Fig. S7). Finally, to further reduce the number of atoms involved in our computations, we discarded those parts of the residue that were not directly involved in the reaction, that is, the adenine ring of the NAD^+ . The cut bonds were replaced by bonds with hydrogen atoms. The size of included amino acid was also reduced by an appropriate cut of conveniently chosen chemical bonds (in particular the bonds involving the C_α atoms). The cut bonds were again replaced by bonds with hydrogen atoms. The full QM model system used in our computations is reported in Supplementary Figure S7.

Emulating the protein environment

To emulate the partially constraining effect of the protein environment, during the geometry optimization, we kept frozen to their crystallographic coordinates the positions of appropriately chosen atoms: these were mainly the hydrogen atoms added in place of the cut bonds and the atoms near the border of the model system and not directly involved in the reaction or in hydrogen bond formation. This approach preserved the geometry of the active site cavity, avoiding the possibility that the secondary structure of the GAPDH active site may run into unwanted conformational changes, and emulated the constraining effect of the protein environment. The frozen atoms are indicated in Supplementary Figure S9.

QM calculations

All reported DFT computations were carried out with the Gaussian 09 series of programs (24) using the M06-2X functional (69, 70). The system was partitioned into two regions, which were assigned as basis sets of different accuracy (8, 12, 13). The atoms of one region were those directly involved in the reaction (*i.e.*, Cys149, H_2O_2 molecule) or in the formation of hydrogen bonds (*i.e.*, His179 side chain): for these atoms, we used the 6-31+G* basis set (24). The other region included all remaining atoms, which were described by the 3-21G* basis set (24). The level of accuracy (basis set) used for the various atoms is schematically indicated in Supplementary Figure S1.

QM/MM calculations and fingerprint analyses

To quantify the catalytic effect of the 10 different residues between AtGAPC1 and AtGAPA in the oxidation of Cys149, we recomputed the energy barriers calculating the electrostatic (Coulomb) effect of the *i*th residue on the QM region in AtGAPC1 and AtGAPA (fingerprint analysis) (14, 54, 55). In each calculation, the QM model (geometries from the previously identified critical points) is surrounded by the atomic point charges (from Amber 10 force field) (15) of the *i*th residue, with the charges placed according to the crystallographic coordinates of the *i*th residue itself. The analyses demonstrate the stabilizing/destabilizing effects exerted by the various residues.

Acknowledgments

This work was supported by FARB 2012, University of Bologna (FARB2012FRAN to M.Z., S.F. and F.S.). We thank the European Synchrotron Radiation Facility (ESRF), Grenoble, France, for synchrotron beam-time allocation (BAG proposal MX1552). S.F. and G.F. thank the Consorzio Interuniversitario di Ricerca in Chimica dei Metalli nei Sistemi Biologici (CIRCSMB).

Author Disclosure Statement

No competing financial interests exist.

References

1. Akter S, Huang J, Bodra N, De Smet B, Wahni K, Rombaut, D, Pauwels J, Gevaert K, Carroll K, Van Breusegem F, and Messens J. DYN-2 Based identification of arabidopsis sulfenomes. *Mol Cell Proteomics* 14: 1183–1200, 2015.
2. Anandakrishnan R, Aguilar B, and Onufriev AV. H++ 3.0: automating pK prediction and the preparation of biomolecular structures for atomistic molecular modeling and simulations. *Nucl Acids Res* 40: 537–541, 2012.
3. Balsera M, Uberegui E, Schürmann P, and Buchanan BB. Evolutionary development of redox regulation in chloroplasts. *Antioxid Redox Signal* 21: 1327–1355, 2014.
4. Battye TG, Kontogiannis L, Johnson O, Powell HR, and Leslie AG. iMOSFLM: a new graphical interface for diffraction-image processing with MOSFLM. *Acta Crystallogr D Biol Crystallogr* 67: 271–281, 2011.
5. Bedhomme M, Adamo M, Marchand CH, Couturier J, Rouhier N, Lemaire SD, Zaffagnini M, and Trost P. Glutathionylation of cytosolic glyceraldehyde-3-phosphate dehydrogenase from the model plant *Arabidopsis thaliana* is reversed by both glutaredoxins and thioredoxins in vitro. *Biochem J* 445: 337–347, 2012.
6. Bedhomme M, Zaffagnini M, Marchand CH, Gao XH, Moslonka-Lefebvre M, Michelet L, Decottignies P, and Lemaire SD. Regulation by glutathionylation of isocitrate lyase from *Chlamydomonas reinhardtii*. *J Biol Chem* 284: 36282–91, 2009.
7. Billiet L, Geerlings P, Messens J, and Roos, G. The thermodynamics of thiol sulfenylation. *Free Radic Biol Med* 52: 1473–1485, 2012.
8. Bottoni A, Miscione GP, and Calvaresi M. Computational evidence for the substrate-assisted catalytic mechanism of O-GlcNAcase. A DFT investigation. *Phys Chem Chem Phys* 20: 9568–9577, 2011.
9. Brünger AT, Adams PD, Clore GM, DeLano WL, Gros P, Grosse-Kunstleve RW, Jiang JS, Kuszewski J, Nilges M, Pannu NS, Read RJ, Rice LM, Simonson T, and Warren GL. Crystallography & NMR system: a new software suite for macromolecular structure determination. *Acta Crystallogr D Biol Crystallogr* 54: 905–921, 1998.
10. Burla MC, Caliendo R, Camalli M, Carrozzini B, Cascarano GL, De Caro L, Giacovazzo C, Polidori G, Siliqi D, and Spagna R. IL MILIONE: a suite of computer programs for crystal structure solution of protein. *J Appl Cryst* 40: 609–613, 2007.
11. Butterfield DA, Hardas SS, and Lange ML. Oxidatively modified glyceraldehyde-3-phosphate dehydrogenase (GAPDH) and Alzheimer's disease: many pathways to neurodegeneration. *J Alzheimers Dis* 20: 369–393, 2010.
12. Calvaresi M, Bottoni A, and Garavelli M. Computational clues for a new mechanism in the glycosylase activity of

- the human DNA repair protein hOGG1. A generalized paradigm for purine-repairing systems? *J Phys Chem B* 111: 6557–6570, 2007.
13. Calvaresi M, Garavelli M, and Bottoni A. Computational evidence for the catalytic mechanism of glutamyl cyclase. A DFT investigation. *Proteins* 73: 527–538, 2008.
 14. Calvaresi M, Stenta M, Garavelli M, Altoé P, and Bottoni A. Computational evidence for the catalytic mechanism of human glutathione S-transferase A3-3: a QM/MM investigation. *ACS Catalysis* 2: 280–286, 2012.
 15. Case DA, Darden TA, Cheatham III TE, Simmerling CL, Wang J, Duke RE, Luo R, Crowley M, Walker RC, Zhang W, Merz KM, Wang B, Hayik S, Roitberg A, Seabra G, Kolossváry I, Wong KF, Paesani F, Vanicek J, Wu X, Brozell SR, Steinbrecher T, Gohlke H, Yang L, Tan C, Mongan J, Hornak V, Cui G, Matthews DH, Seetin MG, Sagui C, Babin V, and Kollman PA. *AMBER 10*. San Francisco: University of California, 2008.
 16. Del Giudice A, Pavel NV, Galantini L, Falini G, Trost P, Fermani S, and Sparla F. Unravelling the shape and structural assembly of the photosynthetic GAPDH–CP12–PRK complex from *Arabidopsis thaliana* by small-angle X-ray scattering analysis. *Acta Crystallogr D Biol Crystallogr* 71: 2372–2385, 2015.
 17. Emsley P and Cowtan K. Coot: model-building tools for molecular graphics. *Acta Crystallogr D Biol Crystallogr* 60: 2126–2132, 2004.
 18. Evans P. Scaling and assessment of data quality. *Acta Crystallogr D Biol Crystallogr* 62: 72–82, 2006.
 19. Fermani S, Sparla F, Marri L, Thumiger A, Pupillo P, Falini G, and Trost P. Structure of photosynthetic glyceraldehyde-3-phosphate dehydrogenase (isoform A4) from *Arabidopsis thaliana* in complex with NAD. *Acta Crystallogr F Struct Biol Cryst Commun* 66: 621–626, 2010.
 20. Fermani S, Trivelli X, Sparla F, Thumiger A, Calvaresi M, Marri L, Falini G, Zerbetto F, and Trost P. Conformational selection and folding-upon-binding of intrinsically disordered protein CP12 regulate photosynthetic enzymes assembly. *J Biol Chem* 287: 21372–21383, 2012.
 21. Ferrer-Sueta G, Manta B, Botti H, Radi R, Trujillo M, and Denicola A. Factors affecting protein thiol reactivity and specificity in peroxide reduction. *Chem Res Toxicol* 24: 434–450, 2011.
 22. Fige RM, Schubert M, Brinkmann H, and Cerff R. Glyceraldehyde-3-phosphate dehydrogenase gene diversity in eubacteria and eukaryotes: evidence for intra- and interkingdom gene transfer. *Mol Biol Evol* 16: 429–440, 1999.
 23. Foyer CH, Lelandais M, and Kunert K-J. Photooxidative stress in plants. *Physiol Plant* 92: 696–717, 1997.
 24. Frisch MJ, Trucks GW, Schlegel HB, Scuseria GE, Robb MA, Cheeseman JR, Scalmani G, Barone V, Mennucci B, Petersson GA, Nakatsuji H, Caricato M, Li X, Hratchian HP, Izmaylov AF, Bloino J, Zheng G, Sonnenberg JL, Hada M, Ehara M, Toyota K, Fukuda R, Hasegawa J, Ishida M, Nakajima T, Honda Y, Kitao O, Nakai H, Vreven T, Montgomery JA, Jr., Peralta JE, Ogliaro F, Bearpark M, Heyd JJ, Brothers E, Kudin KN, Staroverov VN, Kobayashi R, Normand J, Raghavachari K, Rendell A, Burant JC, Iyengar SS, Tomasi J, Cossi M, Rega N, Millam JM, Klene M, Knox JE, Cross JB, Bakken V, Adamo C, Jaramillo J, Gomperts R, Stratmann RE, Yazyev O, Austin AJ, Cammi R, Pomelli C, Ochterski JW, Martin RL, Morokuma K, Zakrzewski VG, Voth GA, Salvador P, Dannenberg JJ, Dapprich S, Daniels AD, Farkas Ö, Foresman JB, Ortiz JV, Cioslowski J, and Fox DJ. Gaussian 09, Revision E01, Gaussian, Inc., Wallingford CT, 2009.
 25. Hall A, Nelson K, Poole LB, and Karplus PA. Structure-based insights into the catalytic power and conformational dexterity of peroxiredoxins. *Antioxid Redox Signal* 15: 795–815, 2011.
 26. Hall A, Parsonage D, Poole LB, and Karplus PA. Structural evidence that peroxiredoxin catalytic power is based on transition-state stabilization. *J Mol Biol* 402: 194–209, 2010.
 27. Hancock JT, Henson D, Nyirenda M, Desikan R, Harrison J, Lewis M, Hughes J, and Neill SJ. Proteomic identification of glyceraldehyde 3-phosphate dehydrogenase as an inhibitory target of hydrogen peroxide in *Arabidopsis*. *Plant Physiol Biochem* 43: 828–835, 2005.
 28. Hildebrandt T, Knuesting J, Berndt C, Morgan B, and Scheibe R. Cytosolic thiol switches regulating basic cellular functions: GAPDH as an information hub? *Biol Chem* 396: 523–537, 2015.
 29. Jeong W, Bae SH, Toledano MB, and Rhee SG. Role of sulfiredoxin as a regulator of peroxiredoxin function and regulation of its expression. *Free Radic Biol Med* 53: 447–456, 2012.
 30. Kitz R and Wilson IB. Esters of methanesulfonic acid as irreversible inhibitors of acetylcholinesterase. *J Biol Chem* 237: 3245–3249, 1962.
 31. Klomsiri C, Karplus PA, and Poole LB. Cysteine-based redox switches in enzymes. *Antioxid Redox Signal* 14: 1065–1077, 2011.
 32. Laskowski RA and Swindells MB. LigPlot+: multiple ligand-protein interaction diagrams for drug discovery. *J Chem Inf Model* 51: 2778–2786, 2011.
 33. Laskowski RA, MacArthur MW, Moss DS, and Thornton JM. PROCHECK: a program to check the stereochemical quality of protein structures. *J Appl Cryst* 26: 283–291, 1993.
 34. Lo Conte M and Carroll KS. The redox biochemistry of protein sulfenylation and sulfinylation. *J Biol Chem* 288: 26480–26488, 2013.
 35. Marri L, Thieulin-Pardo G, Lebrun R, Puppo R, Zaffagnini M, Trost P, Gontero B, and Sparla F. CP12-mediated protection of Calvin-Benson cycle enzymes from oxidative stress. *Biochimie* 97: 228–237, 2014.
 36. Marri L, Trost P, Pupillo P, and Sparla F. Reconstitution and properties of the recombinant glyceraldehyde-3-phosphate dehydrogenase/CP12/phosphoribulokinase supramolecular complex of *Arabidopsis*. *Plant Physiol* 139: 1433–1443, 2005.
 37. Michelet L, Zaffagnini M, Morisse S, Sparla F, Pérez-Pérez ME, Francia F, Danon A, Marchand CH, Fermani S, Trost P, and Lemaire SD. Redox regulation of the Calvin-Benson cycle: something old, something new. *Front Plant Sci* 4: 470, 2013.
 38. Mittler R, Vanderauwera S, Suzuki N, Miller G, Tognetti VB, Vandenpoele K, Gollery M, Shulaev V, and Van Breusegem F. ROS signaling: the new wave? *Trends Plant Sci* 16: 300–309, 2011.
 39. Moras D, Olsen KW, Sabesan MN, Buehner M, Ford GC, and Rossmann MG. Studies of asymmetry in the three-dimensional structure of lobster D-glyceraldehyde-3-phosphate dehydrogenase. *J Biol Chem* 250: 9137–9162, 1975.
 40. Morisse S, Zaffagnini M, Gao XH, Lemaire SD, and Marchand CH. Insight into protein S-nitrosylation in

- Chlamydomonas reinhardtii*. *Antioxid Redox Signal* 21: 1271–1284, 2014.
41. Muthuramalingam M, Matros A, Scheibe R, Mock HP, and Dietz KJ. The hydrogen peroxide-sensitive proteome of the chloroplast in vitro and in vivo. *Front Plant Sci* 4: 54, 2013.
 42. Noctor G, Lelarge-Trouverie C, and Mhamdi A. The metabolomics of oxidative stress. *Phytochemistry* 112: 33–53, 2015.
 43. O'Brien JA, Daudi A, Butt VS, and Bolwell GP. Reactive oxygen species and their role in plant defence and cell wall metabolism. *Planta* 236: 765–779, 2012.
 44. Paulsen CE and Carroll KS. Cysteine-mediated redox signaling: chemistry, biology, and tools for discovery. *Chem Rev* 113: 4633–4679, 2013.
 45. Peralta D, Bronowska AK, Morgan B, Dóka É, Van Laer K, Nagy P, Gräter F, and Dick TP. A proton relay enhances H₂O₂ sensitivity of GAPDH to facilitate metabolic adaptation. *Nat Chem Biol* 11: 156–163, 2015.
 46. Piattoni CV, Guerrero SA, and Iglesias AA. A differential redox regulation of the pathways metabolizing glyceraldehyde-3-phosphate tunes the production of reducing power in the cytosol of plant cells. *Int J Mol Sci* 14: 8073–8092, 2013.
 47. Poole LB and Nelson KJ. Discovering mechanisms of signaling-mediated cysteine oxidation. *Curr Opin Chem Biol* 12: 18–24, 2008.
 48. Rahantaniaina MS, Tuzet A, Mhamdi A, and Noctor G. Missing links in understanding redox signaling via thiol/disulfide modulation: how is glutathione oxidized in plants? *Front Plant Sci* 4: 477, 2013.
 49. Roos G, Foloppe N, and Messens J. Understanding the pK(a) of redox cysteines: the key role of hydrogen bonding. *Antioxid Redox Signal* 18: 94–127, 2013.
 50. Schippers JH, Nguyen HM, Lu D, Schmidt R, and Mueller-Roeber B. ROS homeostasis during development: an evolutionary conserved strategy. *Cell Mol Life Sci* 69: 3245–3257, 2012.
 51. Schmitt FJ, Renger G, Friedrich T, Kreslavski VD, Zhar-mukhamedov SK, Los DA, Kuznetsov VV, and Allakh-verdiev SI. Reactive oxygen species: re-evaluation of generation, monitoring and role in stress-signaling in phototrophic organisms. *Biochim Biophys Acta* 1837: 835–848, 2014.
 52. Sirover MA. New insights into an old protein: the functional diversity of mammalian glyceraldehyde-3-phosphate dehydrogenase. *Biochim Biophys Acta* 1432: 159–184, 1999.
 53. Sparla F, Zaffagnini M, Wedel N, Scheibe R, Pupillo P, and Trost P. Regulation of photosynthetic GAPDH dissected by mutants. *Plant Physiol* 138: 2210–2219, 2005.
 54. Stenta M, Calvaresi M, Altoè P, Spinelli D, Garavelli M, and Bottoni A. The catalytic activity of proline racemase: a quantum mechanical/molecular mechanical study. *J Phys Chem B* 112: 1057–1059, 2008.
 55. Stenta M, Calvaresi M, Altoè P, Spinelli D, Garavelli M, Galeazzi R, and Bottoni A. Catalytic mechanism of diaminopimelate epimerase: a QM/MM investigation. *J Chem Theory Comput* 5: 1915–1930, 2009.
 56. Tien YC, Chuankhayon P, Huang YC, Chen CD, Alikhajeh J, Chang SL, and Chen CJ. Crystal structures of rice (*Oryza sativa*) glyceraldehyde-3-phosphate dehydrogenase complexes with NAD and sulfate suggest involvement of Phe37 in NAD binding for catalysis. *Plant Mol Biol* 80: 389–403, 2012.
 57. Trost P, Fermani S, Marri L, Zaffagnini M, Falini G, Scagliarini S, Pupillo P, and Sparla F. Thioredoxin-dependent regulation of photosynthetic glyceraldehyde-3-phosphate dehydrogenase: autonomous vs. CP12-dependent mechanisms. *Photosynth Res* 89: 263–275, 2006.
 58. van Bergen LA, Roos G, and De Proft F. From thiol to sulfonic acid: modeling the oxidation pathway of protein thiols by hydrogen peroxide. *J Phys Chem A* 118: 6078–6084, 2014.
 59. Wang H, Wang S, Lu Y, Alvarez S, Hicks LM, Ge X, and Xia Y. Proteomic analysis of early-responsive redox-sensitive proteins in Arabidopsis. *J Proteome Res* 11: 412–424, 2012.
 60. Waszczak C, Akter S, Eeckhout D, Persiau G, Wahni K, Bodra N, Van Molle I, De Smet B, Vertommen D, Gevaert K, De Jaeger G, Van Montagu M, Messens J, and Van Breusegem F. Sulfenome mining in arabidopsis thaliana. *Proc Natl Acad Sci U S A* 111: 11545–11550, 2014.
 61. Winterbourn CC. Reconciling the chemistry and biology of reactive oxygen species. *Nat Chem Biol* 4: 278–286, 2008.
 62. Zaffagnini M, Bedhomme M, Groni H, Marchand CH, Puppo C, Gontero B, Cassier-Chauvat C, Decottignies P, and Lemaire SD. Glutathionylation in the photosynthetic model organism *Chlamydomonas reinhardtii*: a proteomic survey. *Mol Cell Proteomics* 11: M111.014142, 2012.
 63. Zaffagnini M, Bedhomme M, Marchand CH, Couturier JR, Gao XH, Rouhier N, Trost P, and Lemaire SD. Glutaredoxin s12: unique properties for redox signaling. *Antioxid Redox Signal* 16: 17–32, 2012.
 64. Zaffagnini M, Bedhomme M, Marchand CH, Morisse S, Trost P, and Lemaire SD. Redox regulation in photosynthetic organisms: focus on glutathionylation. *Antioxid Redox Signal* 16: 567–586, 2012.
 65. Zaffagnini M, Fermani S, Costa A, Lemaire SD, and Trost P. Plant cytoplasmic GAPDH: redox post-translational modifications and moonlighting properties. *Front Plant Sci* 4: 450, 2013.
 66. Zaffagnini M, Michelet L, Marchand C, Sparla F, Decottignies P, Le Marechal P, Miginiac-Maslow M, Noctor G, Trost P, and Lemaire SD. The thioredoxin-independent isoform of chloroplastic glyceraldehyde-3-phosphate dehydrogenase is selectively regulated by glutathionylation. *FEBS J* 274: 212–226, 2007.
 67. Zaffagnini M, Morisse S, Bedhomme M, Marchand CH, Festa M, Rouhier N, Lemaire SD, and Trost P. Mechanisms of nitrosylation and denitrosylation of cytoplasmic glyceraldehyde-3-phosphate dehydrogenase from arabidopsis thaliana. *J Biol Chem* 288: 22777–22789, 2013.
 68. Zeida A, Reyes AM, Lebrero MC, Radi R, Trujillo M, and Estrin DA. The extraordinary catalytic ability of peroxiredoxins: a combined experimental and QM/MM study on the fast thiol oxidation step. *Chem Commun (Camb)* 50: 10070–10073, 2014.
 69. Zhao Y and Truhlar DG. Density functional for spectroscopy: no long-range self-interaction error, good performance for Rydberg and charge-transfer states, and better performance on average than B3LYP for ground states. *J Phys Chem A* 110: 13126–13130, 2006.
 70. Zhao Y and Truhlar DG. The M06 suite of density functionals for main group thermochemistry, thermochemical kinetics, noncovalent interactions, excited states, and transition elements: two new functionals and systematic testing of four M06-class functionals and 12 other functionals. *Theor Chem Account* 120: 215–241, 2008.

Address correspondence to:

Prof. Paolo Trost
Department of Pharmacy and Biotechnology
University of Bologna
Via Irnerio 42
Bologna 40126
Italy

E-mail: paolo.trost@unibo.it

Dr. Mirko Zaffagnini
Department of Pharmacy and Biotechnology
University of Bologna
Via Irnerio 42
Bologna 40126
Italy

E-mail: mirko.zaffagnini3@unibo.it

Date of first submission to ARS Central, June 12, 2015; date of final revised submission, November 6, 2015; date of acceptance, November 26, 2015.

Abbreviations Used

AR/HRP = Amplex Red/horseradish peroxidase
 ASA = accessible surface area
 AtGAPA = photosynthetic isoform of Arabidopsis GAPDH
 AtGAPC1 = glycolytic isoform 1 of Arabidopsis GAPDH
 DTT = dithiothreitol
 GAPDH = glyceraldehyde-3-phosphate dehydrogenase
 GRXs = glutaredoxins
 IAM = iodoacetamide
 NAD = nicotinamide adenine dinucleotide
 PES = potential energy surface
 PGK = phosphoglycerate kinase
 PRX = peroxiredoxin
 QM/MM = quantum mechanical/molecular mechanical
 ROS = reactive oxygen species
 SD = standard deviation
 SRXs = sulfiredoxins
 TS = transition state